Available online at www.sciencedirect.com
SCIENCE DIRECT®
PERGAMON
Polyhedron 22 (2003) 2401–2408
POLYHEDRON
www.elsevier.com/locate/poly

# Vibronic dynamic problem of valence tautomerism in cobalt compounds. Magnetic and optical properties

Sophia I. Klokishner *, O.S. Reu

*State University of Moldova, Mateevich Street 60, Kishinev 2009, Moldova*

Received 20 November 2002; accepted 12 December 2002

**Abstract**

The model employed takes into account the main physical factors responsible for the temperature transformations of optical spectra and magnetic properties: intramolecular transfer of the excess electron, vibronic and exchange interactions. For a single valence tautomeric complex the vibronic problem of pseudo-Jahn-Teller effect is solved. The magnetic moment is shown to increase gradually from $1.73\mu_B$ to $4.34\mu_B$. The spectrum of the isolated complex in the near infrared range is revealed to represent a band related to the light induced transfer of an electron from the catecholate ligand to the metal ion. The suggested model is in qualitative agreement with the experimental data.


*Keywords:* Valence tautomerism; Cobalt; Magnetic moment; Charge-transfer band

## 1. Introduction

Transition metal complexes of Co, Mn, Fe, Rh, Ir and Cu with ligands derived from substituted *o*-benzoquinones show valence tautomerism [1–20]. For Co-complexes the interconversion is described by the equation:

$$[\text{low-spin(ls)-Co}^{3+}(\text{N}\hat{}\text{N})\text{sq}^{1-}\ \text{cat}^{2-}] \leftrightarrow [\text{high-spin(hs)-Co}^{2+}(\text{N}\hat{}\text{N})(\text{sq}^{-1})_2]$$

where N^N is a chelating diiminimum ligand, the ligands semiquinone (sq) and catecholate (cat) can be obtained from *o*-quinone by an addition of one and two electrons to the empty π* molecular orbital [20]. Large changes in optical and magnetic properties are revealed to associate with valence tautomeric transformation. For a complex in solution the valence tautomeric interconversion occurs gradually over a large temperature range of about 100 K, and the magnetic moment increases from $1.73\mu_B$ at low temperatures to $4–4.4\mu_B$ at higher temperatures [20]. With temperature growth in the visible range the absorption spectrum characteristic of the ls-Co(III)-tautomer (ls: low-spin) completely converts to that belonging to the hs-Co(II)-tautomer (hs: high-spin) [16]. At low temperatures in the near infrared region of spectrum of complexes in solution a band appears at 2500 nm [16]. The intensity of this band decreases significantly as the temperature is increased from 15 to 295 K. The nature of this band and the reasons of its temperature transformation have not been revealed yet.

The theoretical description of valence tautomeric systems has been carried out in papers [20,21]. In Ref. [20] with the aid of the density functional method the energy spectrum of the localized states of an isolated cobalt complex with two *o*-quinone derived ligands was obtained. The electron-vibrational coupling, the electron transfer between the cat ligand and the cobalt ion as well as between the cat and sq ligands were not taken into account. Paper [21] was aimed at the elucidation of the role played by intra and intermolecular interactions in magnetic properties of isolated complexes and crystals undergoing valence tautomeric transformation. As distinguished from Ref. [20] the model developed in Ref. [21] involved electron transfer processes, magnetic exchange, vibronic and cooperative interactions. However, the problem was solved in Ref. [21] in the adiabatic approximation. Besides [21], this approach was also

* Corresponding author. Tel.: +373-2-72-0078; fax: +373-2-24-0655.
*E-mail address:* sophia@usm.md (S.I. Klokishner).

0277-5387/03/$ - see front matter 
doi:10.1016/S0277-5387(03)00148-7

used in a number of papers [22–24] and was shown to give good results, when calculating thermodynamic characteristics of systems with labile electronic states. Meanwhile, as is well known the validity of the adiabatic approximation for the optical band problem of electron-vibrational Jahn-Teller systems is restricted to the case of strong vibronic coupling and/or high temperatures. Detailed studies also show that in Jahn-Teller systems some light absorption spectrum regions, for whose calculation the non-adiabatic effects are important, cannot be described even in the favourable case of high temperatures and strong vibronic coupling [25]. A characteristic example are the electron transfer bands in mixed valence systems with double-well adiabatic potentials [26]. Physically similar problems also appear in the description of optical bands arising in the infrared region and related to light-induced electron transfer within a single valence tautomeric molecule so far as in this case the mixing of the tunnel states of the molecule by molecular vibrations results in the pseudo-Jahn-Teller effect. Here we propose a vibronic dynamic model of valence tautomerism in a single molecule. Using it we shall explain the peculiarities of the magnetic properties and describe the optical band within the infrared range. Special attention will be put on the elucidation of the question what type of light-induced electron transfer: cat ligand → Co ion or cat ligand → sq ligand gives rise to the observed band at 2500 nm.

## 2. Hamiltonian of the valence tautomeric molecule

Each valence tautomeric molecule is supposed to consist of a cobalt ion (a) and two ligands b and c (cat and sq or two sq). The ligands are assumed to occupy equivalent positions. The five d-orbitals $\varphi_{a\alpha}$ ($\alpha = 1-5$) of the Co-ion are taken to form two groups (Fig. 1). The energy gap between the group of low-lying orbitals $\varphi_{a3}$, $\varphi_{a4}$, $\varphi_{a5}$ and the higher in energy orbitals $\varphi_{a1}$, $\varphi_{a2}$ will be considered well above than the separation of states in each group. The six electrons of the ls-Co(III)-ion are paired up in the orbitals $\varphi_{a\alpha}$ ($\alpha = 3-5$) (Fig. 1(a)). The unpaired electron in the ls-Co(II)-ion may occupy either of the two orbitals $\varphi_{a1}$ or $\varphi_{a2}$ (Fig. 1(b)). The lowest in energy occupation schemes for the hs-Co(II)-ion look as follows: two of the low-lying orbitals $\varphi_{a\alpha}$ ($\alpha = 3-5$) are doubly occupied and the other three orbitals are singly occupied (Fig. 1(c)). For the ligands the only molecular orbital $\psi_d$ (d = b, c) is taken into account (Fig. 1(d and e)).

The Hamiltonian of an isolated molecule is written in the form:

$$h = H_e + H_L + H_{eV} \quad (1)$$

where $H_e$ is the electronic Hamiltonian determining the wave functions and the eigenvalues of a molecule in the

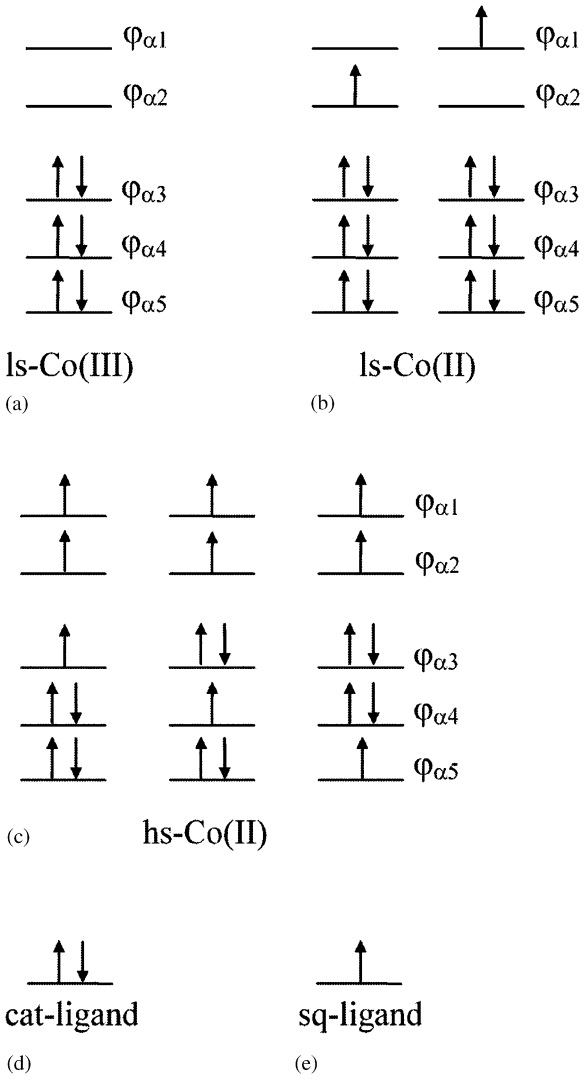


Fig. 1. Schemes of orbitals for the Co-ion and *o*-quinone derived ligands. (a) ls-Co(III)-ion, (b) ls-Co(II)-ion, (c) hs-Co(II)-ion, (d) cat-ligand, (e) sq-ligand.

fixed nuclear configuration, the Hamiltonian $H_e$ contains the kinetic and potential energies of all electrons as well as their interelectronic repulsion. $H_L$ is the Hamiltonian of free lattice vibrations and $H_{eV}$ is the Hamiltonian of vibronic interaction. As a basis set we take the states of a molecule with localized electrons arising from its four configurations [21]:

I. ls-Co(III)(*a*), cat(*b*), sq(*c*);

II. ls-Co(III)(*a*), sq(*b*), cat(*c*);

III. ls-Co(II)(*a*), sq(*b*), sq(*c*);

IV. hs-Co(II)(*a*), sq(*b*), sq(*c*) (2)

For the construction of the electronic wave functions of the localized molecular states the following spin coupling scheme is applied

$$\vec{S}_a + \vec{S}_b = \vec{S}_{ab}, \quad \vec{S}_{ab} + \vec{S}_c = \vec{S} \quad (3)$$

where $S$ is the total spin of the molecule, $S_{ab}$ is the intermediate spin, $S_a$, $S_b$, $S_c$ are the individual spins of the Co-ion and the ligands, respectively. In the accepted spin-addition scheme the general form of the electronic molecular wave functions can be presented as follows:

$$|j(\alpha)S(S_{ab})M\rangle = \sum_{\substack{m_a,m_b\\ m_c,m_{ab}}} C^{S_{ab}m_{ab}}_{S_am_aS_bm_b} C^{SM}_{S_{ab}m_{ab}S_cm_c}$$

$$|\Phi^{j(\alpha)}_a(S_am_a)\Phi^j_b(S_bm_b)\Phi^j_c(S_cm_c)| \tag{4}$$

here $j = 1$–4 refers to the configuration (Eq. (2)) from which the state originates, $M$ is the projection of the full spin $S$, $S = 1/2$ for $j = 1$, 2, $S = 1/2$, 1/2, 3/2 for $j = 3$ and $S = 1/2$, 3/2, 3/2, 5/2 for $j = 4$, $\alpha = 0$ for unique states arising from configurations I and II ($j = 1$, 2), but for $j = 3$, $\alpha = 1$, 2 and corresponds to the label of the d-orbital with the unpaired electron in the ls-Co(II)-ion (Fig. 1(b)). Analogously, for $j = 4$ $\alpha$ acquires the values 3–5 that point out to the singly occupied d-orbital of the lower group of orbitals in the hs-Co(II)-ion (Fig. 1(c)). Finally, $m_a$, $m_b$, $m_c$, $m_{ab}$ are the projections of spins $S_a$, $S_b$, $S_c$, $S_{ab}$, respectively, $C^{S_3m_3}_{S_1m_1S_2m_2}$ are the Clebsch–Gordon coefficients, $\Phi^{j(\alpha)}_a(S_am_a)$ and $\Phi^j_d(S_dm_d)$ ($d = b$, $c$) are the wave functions of the Co-ion and the ligands complying with the configuration $j$. The evident form of these wave functions is listed in Ref. [21]. With the aid of wave functions (Eq. (4)) the matrix elements of operators $H_e$ and $H_{eV}$ were calculated. One can find the detailed description of the calculation procedure in Ref. [21]. In the basis of the states $|j(\alpha)S(S_{ab})M\rangle$ only the following matrix elements of the operator $H_e$ are non-zero:

$$\begin{aligned}
&\langle j(\alpha)S(S_{ab})M|H_e|j(\alpha)S(S_{ab})M\rangle = \Delta_j - J_j(S(S+1)\\
&\quad -S_a(S_a+1) - S_b(S_b+1) - S_c(S_c+1)),\\
&\quad (j = 3,\ 4),\\
&\langle 1(0)1/2(0)M|H_e|3(\alpha)1/2(0)M\rangle = t_1,\\
&\langle 2(0)1/2(1/2)M|H_e|3(\alpha)1/2(0)M\rangle = -\frac{t_1}{2},\\
&\langle 2(0)1/2(1/2)M|H_e|3(\alpha)1/2(1)M\rangle = -\frac{\sqrt{3}}{2}t_1,\\
&\langle 1(0)1/2(0)M|H_e|2(0)1/2(1/2)M\rangle = t_2
\end{aligned} \tag{5}$$

here $\Delta_3$ and $\Delta_4$ are the energies of the states $|3(\alpha)S(S_{ab})M\rangle$ ($\alpha = 1$, 2) and $|4(\alpha)S(S_{ab})M\rangle$ ($\alpha = 3$–5) with allowance only for crystal-field splitting and intra and intercenter Coulomb interactions, these energies are counted off from the energy of the states $|j(0)1/2(S_{ab})M\rangle$ ($j = 1$, 2), $J_3$ and $J_4$ are the multi-electronic exchange parameters for states of configurations III and IV, respectively. The parameters $t_1$ and $t_2$ describe the electron transfer from the $cat^{2-}$ ligand to the ls-Co(II)-ion and from the $cat^{2-}$ to $sq^{1-}$ ligand [21]. As in Ref. [21] we only take into account the interaction of the Co-ion with the local full-symmetric (breathing) $A_1$-mode. Reading of the vibrational coordinate $Q$ from its equilibrium position in the states $|j(0)1/2(S_{ab})M\rangle$ ($j = 1$, 2) we write the operator of the linear electron-vibrational interaction in the following form [21]:

$$H_{eV} = (V(\vec{r}) - \upsilon)(Q - Q_0) \equiv V'(\vec{r})q \tag{6}$$

here $\vec{r}$ represents the set of electronic coordinates of the Co-ion, $\upsilon = \langle j(0)1/2(S_{ab})M|V(\vec{r})|j(0)1/2(S_{ab})M\rangle$, $Q_0 = -\upsilon/\hbar\omega$, ($j = 1$, 2), $\omega$ is the vibrational frequency. The matrix elements of the operator $V'(\vec{r})$ are expressed as follows [21]:

$$\begin{aligned}
&\langle j(0)1/2(S_{ab})M|V'(\vec{r})|j(0)1/2(S_{ab})M\rangle = 0, \quad (j = 1,\ 2),\\
&\langle j(\alpha)S(S_{ab})M|V'(\vec{r})|j(\alpha)S'(S'_{ab})M'\rangle\\
&\quad = \upsilon_j\delta_{\alpha\alpha'}\delta_{S_{ab}S'_{ab}}\delta_{SS'}\delta_{MM'},\\
&\quad (j = 3,\ 4)
\end{aligned} \tag{7}$$

Finally,

$$H_L = \frac{\hbar\omega}{2}\left(q^2 - \frac{\partial^2}{\partial q^2}\right) \tag{8}$$

From Eqs. (5) and (7) it follows that the states $|3(\alpha)3/2(1)M\rangle$ and $|4(\alpha)S(S_{ab})M\rangle$ represent the eigenstates of the electronic Hamiltonian $H_e$ and are not mixed by the vibronic interaction either with each other or with other states. The solution of the vibronic problem for these states is trivial:

$$\begin{aligned}
&e_1\left(\frac{3}{2},\ n\right) = \Delta_3 - \frac{3}{2}J_3 - \frac{\upsilon_3^2}{2\hbar\omega} + \hbar\omega\left(n + \frac{1}{2}\right), \quad (g_1 = 8),\\
&e_2\left(\frac{1}{2},\ n\right) = \Delta_4 + \frac{9}{2}J_4 - \frac{\upsilon_4^2}{2\hbar\omega} + \hbar\omega\left(n + \frac{1}{2}\right), \quad (g_2 = 6),\\
&e_3\left(\frac{3}{2},\ n\right) = \Delta_4 + \frac{3}{2}J_4 - \frac{\upsilon_4^2}{2\hbar\omega} + \hbar\omega\left(n + \frac{1}{2}\right), \quad (g_3 = 24),\\
&e_4\left(\frac{5}{2},\ n\right) = \Delta_4 - \frac{7}{2}J_4 - \frac{\upsilon_4^2}{2\hbar\omega} + \hbar\omega\left(n + \frac{1}{2}\right),\\
&\quad (g_4 = 18)
\end{aligned} \tag{9}$$

where the numbers $g_i$ indicate both the spin and the orbital degeneracy of the molecular states, $n$ is the quantum number of the harmonic oscillator. In turn, the six states $|j(0)1/2(S_{ab})M\rangle$ and $|3(\alpha)1/2(S_{ab})M\rangle$ are connected by electron transfer. Each of them interacts with full- symmetric vibrations. As a result the pseudo-Janh-Teller problem arises. The hybrid vibronic wave functions corresponding to the dynamic vibronic problem are written as the expansions over the unperturbed electronic ($|j(\alpha)1/2(S_{ab})M\rangle$, $j = 1$, 2, 3) and vibrational states:

$$\Phi_{vM}(\vec{r},\ q) = \sum_{n=0}^{\infty}\sum_{i=1}^{6}\chi_n(q)C^i_{vn}|iM\rangle$$
$$= \sum_{n=0}^{\infty}\chi_n(q)(C^1_{vn}|1(0)1/2(0)M\rangle + C^2_{vn}|2(0)1/2(1/2)M\rangle + C^3_{vn}|3(1)1/2(0)M\rangle + C^4_{vn}|3(1)1/2(1)M\rangle + C^5_{vn}|3(2)1/2(0)M\rangle + C^6_{vn}|3(2)1/2(1)M\rangle) \quad (10)$$

here $\chi_n(q)$ denotes the harmonic oscillator wave-functions and the index $v$ indicates the hybrid states of the valence tautomeric molecule. For numerical calculations of the eigenvalues and eigenvectors of the vibronic dynamic problem 60 unperturbed oscillator states were taken into account (general dimension of the vibronic matrix $360 \times 360$). For given below parameter values increasing the number of basic states does not lead to any change in the energy of the lowest 60 vibronic states, which means that the dimension of the adopted basis set is sufficiently large.

## 3. Magnetic moment

The Van Vleck equation

$$\mu^2 = g^2\mu_B^2\frac{\sum_{i,S} g_i S(S+1)\exp[-E_i(S)/kT]}{\sum_{i,S} g_i \exp[-E_i(S)/kT]} \quad (11)$$

and the electron-vibrational levels obtained by diagonalization of Hamiltonian (Eq. (1)) are used for calculation of the magnetic moment of the valence tautomeric molecule. As a matter of fact, Eq. (11) contains the summation over the hybrid levels $E_v(1/2)$ corresponding to the hybrid wave functions (Eq. (10)) as well as the summation over the pure vibrational levels $e_i(S,n)$ (Eq. (9)) arising from the localized states $|3(\alpha)3/2(1)M\rangle$ and $|4(\alpha)S(S_{ab})M\rangle$. After substitution Eq. (9) in Eq. (11) the expression for $\mu^2$ appears as follows:

$$\mu^2 = \frac{g^2\mu_B^2}{z}\left(\frac{3}{2}\sum_v \exp\left[-\frac{E_v(1/2)}{kT}\right] + \frac{1}{\sinh\left[\frac{\hbar\omega}{2kT}\right]}\left(15\exp\left[-\frac{e_1(3/2)}{kT}\right] + \frac{9}{4}\exp\left[-\frac{e_2(1/2)}{kT}\right] + 45\exp\left[-\frac{e_3(3/2)}{kT}\right] + \frac{315}{4}\exp\left[-\frac{e_4(5/2)}{kT}\right]\right)\right),$$

$$z = 2\sum_v \exp\left[-\frac{E_v(1/2)}{kT}\right] + \frac{1}{\sinh\left[\frac{\hbar\omega}{2kT}\right]} \times \left(4\exp\left[-\frac{e_1(3/2)}{kT}\right] + 3\exp\left[-\frac{e_2(1/2)}{kT}\right] + 12\exp\left[-\frac{e_3(3/2)}{kT}\right] + 9\exp\left[-\frac{e_4(5/2)}{kT}\right]\right) \quad (12)$$

$$e_i(S) = e_i(S,\ n) - \hbar\omega(n+1/2) \quad (13)$$

For the calculation of the temperature dependence of the magnetic moment the following key parameters were used: $\upsilon_3 = 1050\ \mathrm{cm}^{-1}$, $\upsilon_4 = 1575\ \mathrm{cm}^{-1}$, $J_3 = 40\ \mathrm{cm}^{-1}$, $J_4 = 30\ \mathrm{cm}^{-1}$, $\Delta_3 = 1145\ \mathrm{cm}^{-1}$, $\Delta_4 = 2018\ \mathrm{cm}^{-1}$, $t_1 = 1075\ \mathrm{cm}^{-1}$, $t_2 = 73\ \mathrm{cm}^{-1}$, $\hbar\omega = 390\ \mathrm{cm}^{-1}$ (Fig. 2, curves 1, 2). The values of the parameters $\upsilon_j$, $J_j$, $\Delta_j$, ($j = 3, 4$), $t_1$, $t_2$ are close to those estimated in Ref. [21] from the crystal field model and experimental data. The variable temperature magnetic moment is depicted in Fig. 2. It is seen that with temperature rise the magnetic moment increases gradually from $1.73\mu_B$ to $4.34\mu_B$ (Fig. 2, curve 1). The valence tautomeric interconversion takes place in temperature range of about 100 K. The essence of this result is clear from the adiabatic potential scheme (Fig. 3). The numbering of the adiabatic potential branches $U_i(S_i|q)$ coincides with that given in Ref. [21], wherein the analytical expressions for $U_i(S|q)$ were derived. The sheets $U_i(S_i|q)$ ($i = 6$–$9$) have an oscillator shape and correspond to the localized states $|3(\alpha)3/2(1)M\rangle$ and $|4(\alpha)S(S_{ab})M\rangle$. For these states the electron-vibrational levels represent pure harmonic oscillator levels (Eq. (9), Fig. 3). The shape of the adiabatic curves $U_i(1/2|q)$ ($i = 1$–$5$) is not parabolic. These curves originate from the states $|j(0)1/2(S_{ab})M\rangle$ ($j = 1, 2$) and $|3(\alpha)1/2(S_{ab})M\rangle$ coupled by electron transfer. As it was said above the numerical diagonalization of the total Hamiltonian $h$ (Eq. (1)) in the basis of the states $|j(0)1/2(S_{ab})M\rangle$ ($j = 1, 2$) and $|3(\alpha)1/2(S_{ab})M\rangle$ gives the vibronic levels with the energies $E_v(1/2)$. From Fig. 3 it is seen that the lower three vibronic levels are approximately equidistant and similar to the harmonic oscillator energy levels. In the higher vibronic states the electronic and nuclear states are completely mixed, and their spectrum cannot be interpreted in a simple way. For given parameter values the minimum of the adiabatic potential sheet $U_4(1/2|q)$ is the lowest one, and it is followed by the minima of the sheets $U_9(5/2|q)$, $U_8(3/2|q)$, $U_7(1/2|q)$. The ground vibronic level ($E_0(1/2)$) possesses the spin 1/2, and therefore the low temperature limit of the magnetic moment is $1.73\mu_B$ (Fig. 2, curve 1). The magnetic moment retains the value $\mu < 2\mu_B$ up to $T = 120$ K

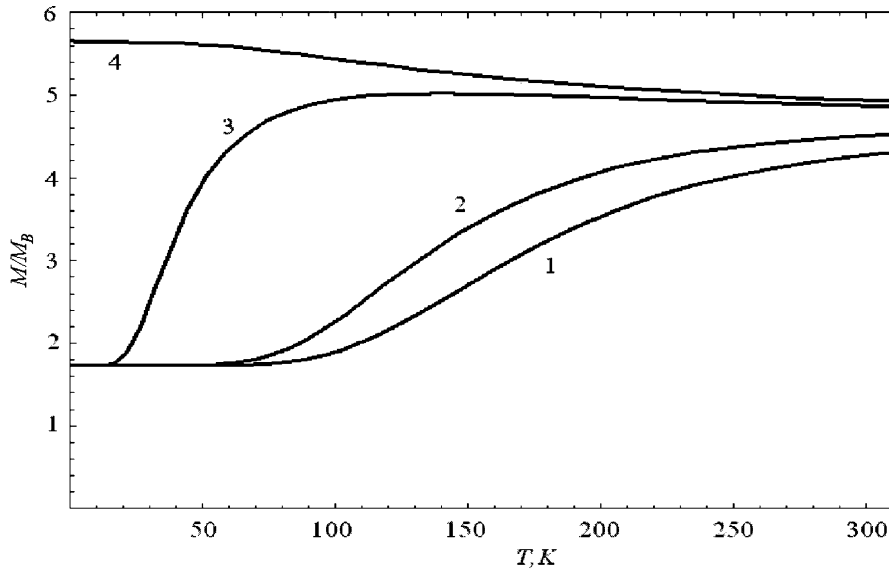


Fig. 2. Plot of the magnetic moment versus temperature for the parameters: $\Delta_3 = 1145\ cm^{-1}$, $\Delta_4 = 2018\ cm^{-1}$, $\upsilon_3 = 1050\ cm^{-1}$, $\upsilon_4 = 1575\ cm^{-1}$, $J_3 = 40\ cm^{-1}$, $J_4 = 30\ cm^{-1}$, $\hbar\omega = 390\ cm^{-1}$, $t_2 = 73\ cm^{-1}$; (1, 2) $t_1 = 1075\ cm^{-1}$; (3) $t_1 = 850\ cm^{-1}$; (4) $t_1 = 800\ cm^{-1}$. The curves 1 and 2 were calculated in the vibronic-dynamic and semiclassical models, respectively.

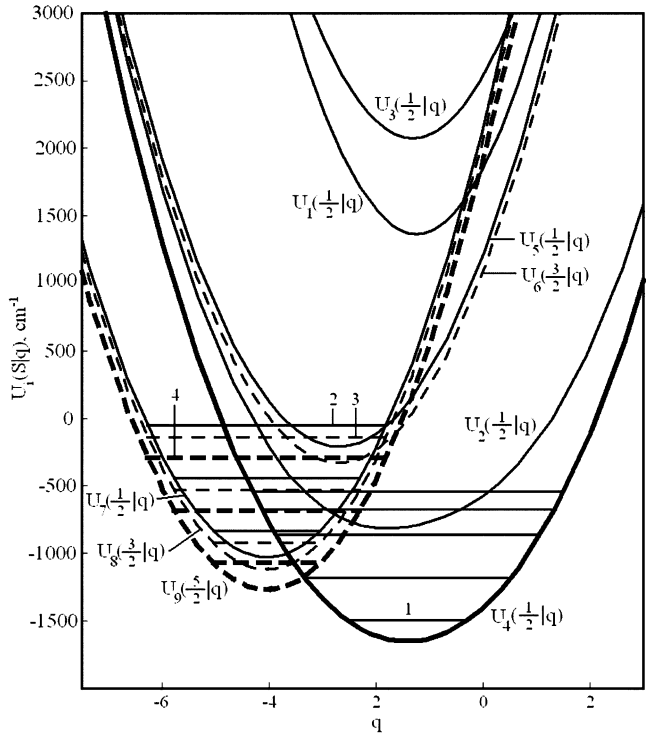


Fig. 3. The adiabatic potentials of an isolated complex in the case of the parameters: $\Delta_3 = 1145\ cm^{-1}$, $\Delta_4 = 2018\ cm^{-1}$, $t_1 = 1075\ cm^{-1}$, $t_2 = 73\ cm^{-1}$, $J_3 = 40\ cm^{-1}$, $J_4 = 30\ cm^{-1}$, $\upsilon_3 = 1050\ cm^{-1}$, $\upsilon_4 = 1575\ cm^{-1}$, $\hbar\omega = 390\ cm^{-1}$; (1) hybrid vibronic levels with $v = 0$–4-thick solid lines, (2, 3, 4) harmonic oscillator levels for $n = 0, 1, 2$; (2) $e_2(1/2, n)$-thin solid line, (3) $e_3(3/2, n)$-thin dashed line, (4) $e_4(5/2, n)$-thick dashed line.

(curve 1) and this is confirmed by experiment [16,20]. Then with temperature rise the levels with the energies $E_1(1/2)$ and $e_4(5/2, 0)$ are populated, and the magnetic moment increases significantly. The obtained values of the magnetic moment at low and high temperatures as well as the width of the temperature range wherein the transformation occurs are close to experimental ones. A more precise fitting of experimental data for the problem with eight parameters $t_1$, $t_2$, $\Delta_j$, $\upsilon_j$, $J_j$ ($j = 3$, 4) seems to be excessively flexible. For comparison in Fig. 2 the magnetic moment curve obtained in the semiclassical approximation is also shown (curve 2). We notice that in the adiabatic approach the low temperature limit $\mu(0) = 1.73\mu_B$. One can also see that for temperatures $T < 70$ K the magnetic moment values calculated in the vibronic dynamic and adiabatic models are the same. Beginning from $T = 70$ K the curve obtained in the semiclassical approach lies higher. The maximum discrepancy takes place in the range $120 < T < 220$. However, the difference between the magnetic moment values obtained in both models is less than 22.3%. At temperatures $T > 220$ the curves draw together. Curves 3 and 4 in Fig. 2 are calculated with the same parameters $\Delta_j$, $\upsilon_j$, $J_j$, $t_2$ as curves 1 and 2, but for the transfer parameter $t_1$ smaller values are taken. For the value $t_1 = 850\ cm^{-1}$ the magnetic moment increases abruptly (Fig. 2, curve 3), because the gap between the minima of the sheets $U_4(1/2|q)$ and $U_9(5/2|q)$ decreases. For the parameter $t_1 = 800\ cm^{-1}$ (Fig. 2, curve 4) the minimum of the adiabatic potential sheet $U_9(5/2|q)$ becomes lower than that of the sheet $U_4(1/2|q)$, the level $e_4(5/2, 0)$ is the ground one, and the low temperature limit of the magnetic moment corresponds to the spin $S = 5/2$.

## 4. Charge-transfer band

The shape of the charge-transfer band arising under absorption of unpolarized light is described by the equation:

$$F(\Omega)=\frac{1}{2}\sum_{M,M'}\sum_{v>v'}\sum_{v'}\frac{N_{v'}-N_v}{z}\rho_{vv'}(\Omega)\overline{|\langle\Phi_{vM}|d_xe_x+d_ye_y|\Phi_{v'M'}\rangle|^2} \quad (14)$$

here $N_v=2\exp[-E_v(1/2)/kT]$ is the equilibrium population of the $v$th vibronic level, the partition function $z$ is determined by Eq. (12), $\rho_{vv'}(\Omega)$ is the line shape connected with the transition between hybrid vibronic states $v$ and $v'$. This line shape is assumed to be Gaussian:

$$\rho_{vv'}(\Omega)=\frac{1}{\sqrt{2\pi}\lambda}\exp\left[-\frac{(E_v-E_{v'}-\hbar\Omega)^2}{2\lambda^2}\right] \quad (15)$$

To smooth the quantum discrete structure of the entire band the second moment of the individual line $\lambda$ should be comparable with the $\hbar\omega$ value. As well as in Ref. [26] we put here $\lambda=\hbar\omega=390\ \mathrm{cm}^{-1}$. Finally, $e_\alpha$ and $d_\alpha$ ($\alpha=x, y$) are the components of the polarization and dipole moment vectors, respectively. The symbol $|\langle\ldots\rangle|^2$ means the averaging over the light polarization. Eq. (14) only accounts for optical transitions between hybrid states $v$ because in the $|j(\alpha)S(S_{ab})M\rangle$ basis the operators $d_x$ and $dy$ have only non-vanishing diagonal matrix elements. Substituting Eq. (10) into Eq. (14) and carrying out the averaging over the light polarization one obtains

$$F(\Omega)=\frac{1}{3}\sum_{v>v'}\sum_{v'}\sum_{n,n'}\sum_{i,i'}\frac{(N_{v'}-N_v)}{z}\rho_{vv'}(\Omega)C^i_{vn}C^{i'}_{vn'}C^i_{v'n}C^{i'}_{v'n'}(d^{ii}_xd^{i'i'}_x+d^{ii}_yd^{i'i'}_y) \quad (16)$$

where the matrix elements $d^{ii}_x$ and $d^{ii}_y$ are given in Ref. [21]. For numerical calculations of the absorption coefficient the transitions between 70 lowest states were calculated (the full number of transitions taken into account was 2485). The temperature dependence of the absorption coefficient $K(\Omega)\sim\Omega F(\Omega)$ is presented in Fig. 4. For all temperatures the charge-transfer band remains essentially asymmetric and possesses a shoulder in the high-frequency range ($\lambda=2000$) as well as a long tail in the low-frequency range. Meanwhile the position of the band maximum at $\lambda_m=2500$ nm remains unchanged with temperature rise. For the absorption band at $T=295$ K two curves are shown in Fig. 4. The first of them accounts for all possible optical transitions between the 70 hybrid states taken into consideration, while the second one is calculated with the allowance only of the transitions between the ground vibronic state and the excited ones. We see, that the contribution of the optical transitions between the excited hybrid states even at $T=295$ K is less than 24% in area and amounts

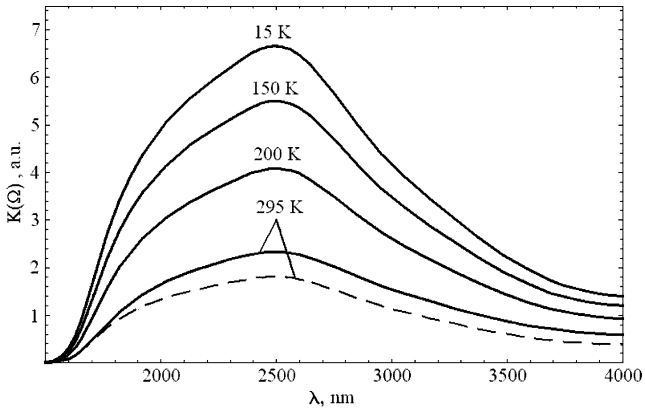


Fig. 4. Temperatures dependence of the absorption coefficient for the parameters: $\Delta_3=1145\ \mathrm{cm}^{-1}$, $\Delta_4=2018\ \mathrm{cm}^{-1}$, $t_1=1075\ \mathrm{cm}^{-1}$, $t_2=73\ \mathrm{cm}^{-1}$, $J_3=40\ \mathrm{cm}^{-1}$, $J_4=30\ \mathrm{cm}^{-1}$, $\upsilon_3=1050\ \mathrm{cm}^{-1}$, $\upsilon_4=1575\ \mathrm{cm}^{-1}$, $\varphi=130^\circ$, $\hbar\omega=390\ \mathrm{cm}^{-1}$. $T=295$ K: dashed line-contribution to the band shape of the optical transitions between the ground hybrid state and excited ones.

to 22,5% in the band maximum height. When decreasing temperature, this contribution falls because of the decrease in the populations of excited states. With temperature rise the intensity of the charge-transfer band diminishes. However, the difference in the intensity of the band at temperatures 15 and 150 K is not significant. Ranging from 150 K a noticeable decrease in the band intensity is observed. Finally, at 295 K the height of the band maximum at 2500 nm becomes 2, 8 times smaller than that at 15 K. The peculiarities of the temperature behaviour of the charge-transfer band can be explained as follows. In the temperature range 15–70 K the lowest two vibronic levels with $v=0$ and 1 corresponding to $S=1/2$ are mainly populated. Therefore at these temperatures the charge-transfer band has its maximum intensity, while the magnetic moment acquires its minimum value $1.73\mu_B$ (Fig. 2, curve 1). With temperature increase the harmonic oscillator levels with spins 5/2, 3/2, 1/2 start populating. A redistribution in the population of the states with different spin values takes place. So far as the degeneracies $g_i$ of the oscillator levels $e_i(S/n)$ with $i=3$, 4 (Eq. (9)) are high in comparison with the degeneracy $g_v=2$ of the hybrid levels $v$, the relative Boltzman population of the latter ones $N_v/z$ decreases with temperature. This results in the fall of the intensity of the charge-transfer band (see Eq. (14)). It should be stressed that the obtained temperature dependence of the charge-transfer band is in accordance with that of the magnetic moment so far as the temperature increase of the magnetic moment (Fig. 2, curve 1) indicates on the population of the harmonic oscillator levels $e_i(S,0)$ ($i=3$, 4) with higher spin values.

If the transfer parameter $t_1$ is decreased (Fig. 5), but all other parameters are taken the same as in Figs. 2–4, for $T=15$ K the intensity of the band at 2500 nm

vanishes. For instance, for $t_1 = 800\ cm^{-1}$ the ground is the harmonic oscillator level $e_4(5/2, 0)$ and the populations of all other states at 15 K are negligible. Therefore $K(\Omega)$ turns to zero. This result does not contradict the temperature dependence of the magnetic moment, for $t_1 = 800\ cm^{-1}$, $\mu(0) = \sqrt{35}\mu_B$ (Fig. 2, curve 4). On the other hand, for $t_1 = 0\ cm^{-1}$ and $t_2 = 1300\ cm^{-1}$ a band with a negligible intensity can be obtained. Meanwhile, the overlap of the orbitals of the Co-ion and of the ligands is far stronger than the overlap of the orbitals of the ligands *b* and *c* [21], consequently, the parameter $t_1$ is well above than the parameter $t_2$, so that the value $t_2 = 1300\ cm^{-1}$ is set too high for the problem under consideration. All above said allows us to assume that the band at 2500 nm appears mainly from the light induced electron transfer between the cat ligand and the Co-ion (Fig. 4). It should be also mentioned that the temperature behaviour of the charge-transfer band presented in Fig. 4 resembles the experimental one obtained in paper [16].

## 5. Concluding remarks

We have considered the problem of valence tautomeric transformation in an isolated complex. In the case of comparable parameters of vibronic interaction and metal–ligand electron transfer the adiabatic approach proves to be invalid for the description of the charge-transfer band in the near infrared range. So far as the localized molecular states arising from configurations [ls-Co(III), cat, sq] and [ls-Co(II), sq, sq] are coupled by electron transfer the dynamic pseudo-Jahn-Teller problem appears. Solving this problem, we have obtained the temperature dependence of the shape of the charge-transfer band as well as of the molecular magnetic moment. The calculations carried out show that the optical band in the infrared range may be assigned to light-induced electron transfer from the cat ligand to the Co-ion. At the same time the suggested model reproduces the course of the temperature dependence of the absorption spectrum in the infrared range. The comparison of the magnetic moment curves obtained in the vibronic dynamic and semiclassical models demonstrates that in a sufficiently wide temperature range the latter model provides quite a good description of the magnetic properties. It is worth nothing that the developed vibronic approach makes it possible to explain simultaneously the spectroscopic and magnetic characteristics of a single valence tautomeric molecule. However, it should be noted that the valence tautomeric transformation is always accompanied by the change of the vibrational frequency (frequency effect) [27]. This effect arises from quadratic electron-vibrational interaction and was analysed for spin crossover systems in our paper [27]. In future we are going to extend the model suggested in Ref. [27] to valence tautomeric systems. It should be also mentioned that during the valence tautomeric transformation the ligand–metal distance changes appreciably with temperature increase. This effect leads to the temperature dependent vibronic coupling parameters and also needs a special consideration. The other problem we are going to address in future is the spin–orbital interaction, however, it is known to be sufficiently reduced for Co-complexes with ligands derived from substituted *o*-benzoquinones [20].

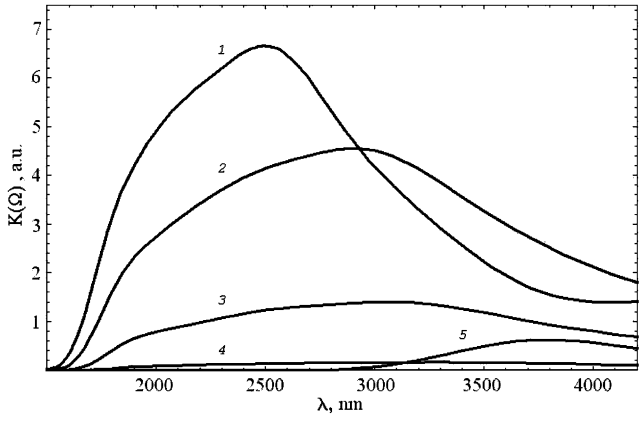


Fig. 5. Absorption coefficient as a function of transfer parameters: $T = 15$ K, $\Delta_3 = 1145\ cm^{-1}$, $\Delta_4 = 2018\ cm^{-1}$, $J_3 = 40\ cm^{-1}$, $J_4 = 30\ cm^{-1}$, $\upsilon_3 = 1050\ cm^{-1}$, $\upsilon_4 = 1575\ cm^{-1}$, $\varphi = 130°$, $\hbar\omega = 390\ cm^{-1}$. (1) $t_1 = 1075\ cm^{-1}$, $t_2 = 73\ cm^{-1}$; (2) $t_1 = 900\ cm^{-1}$, $t_2 = 73\ cm^{-1}$; (3) $t_1 = 850\ cm^{-1}$, $t_2 = 73\ cm^{-1}$; (4) $t_1 = 800\ cm^{-1}$, $t_2 = 73\ cm^{-1}$; (5) $t_1 = 0\ cm^{-1}$, $t_2 = 1300\ cm^{-1}$.

## Acknowledgements

The authors would like to express their gratitude to MRDA/CRDF (Award MP2-3022) and Supreme Council of Science and Technological Development of Moldova (grant 111) for financial support.

## References

[1] R.M. Buchanan, C.G. Pierpont, J. Am. Chem. Soc. 102 (1980) 4951.
[2] (a) D.M. Adams, A. Dei, A.L. Rheingold, D.N. Hendrickson, Angew. Chem. 105 (1993) 954;
(b) D.M. Adams, A. Dei, A.L. Rheingold, D.N. Hendrickson, Angew. Chem., Int. Ed. Engl. 32 (1993) 880.
[3] D.M. Adams, A. Dei, A.L. Rheingold, D.N. Hendrickson, J. Am. Chem. Soc. 115 (1993) 8221.
[4] G.A. Abakumov, V.K. Chercasov, M.P. Bubnov, O.G. Ellert, Z.B. Dobrokhotova, L.N. Zakharov, Y.T. Struchov, Dokl. Akad. Nauk USSR 328 (1993) 12.
[5] O.S. Jung, C.G. Pierpont, Inorg. Chem. 33 (1994) 2227.
[6] M.W. Lynch, D.N. Hendrickson, B.J. Fitzgerald, C.G. Pierpont, J. Am. Chem. Soc. 106 (1984) 2041.
[7] A.S. Attia, C.G. Pierpont, Inorg. Chem. 34 (1995) 1172.

[8] M.W. Lynch, M. Valentine, D.N. Hendrickson, J. Am. Chem. Soc. 104 (1982) 6982.
[9] S.A. Attia, S. Bhattacharya, C.G. Pierpont, Inorg. Chem. 34 (1995) 4427.
[10] A.S. Attia, O.S. Jung, C.G. Pierpont, Inorg. Chem. Acta 226 (1994) 91.
[11] G.A. Abakumov, V.A. Garnov, V.I. Nevodchikov, V.K. Cherkasov, Dokl. Akad. Nauk USSR 304 (1989) 107.
[12] G.A. Abakumov, G.A. Razuvaev, V.I. Nevodchikov, V.K. Cherkasov, J. Organomet. Chem. 341 (1988) 485.
[13] C. Roux, D. Adams, J.P. Itié, A. Polian, D.N. Hendrickson, M. Verdaguer, Inorg. Chem. 35 (1996) 2846.
[14] C.G. Pierpont, C.W. Lange, Progr. Coord. Chem. 41 (1993) 381.
[15] (a) D.M. Adams, B. Li, J.D. Simon, D.N. Hendrickson, Angew. Chem. 107 (1995) 1580;
(b) D.M. Adams, B. Li, J.D. Simon, D.N. Hendrickson, Angew. Chem., Int. Ed. Engl. 34 (1995) 1481.
[16] D.M. Adams, D.N. Hendrickson, J. Am. Chem. Soc. 118 (1996) 11515.
[17] P. Guetlich, A. Dei, Angew. Chem., Int. Ed. Engl. 36 (1997) 2734.
[18] C.G. Pierpont, R.M. Buchanan, Coord. Chem. Rev. 38 (1981) 45.
[19] D.N. Hendrickson, D.M. Adams, in: O. Kahn (Ed.), Magnetism: A. Supramolecular Function, Kluwer, Dordrecht, 1996, p. 357.
[20] D.M. Adams, L. Noodleman, D.N. Hendrickson, Inorg. Chem. 36 (1997) 3966.
[21] S. Klokishner, Chem. Phys. 269 (2001) 411.
[22] B.S. Tsukerblat, S.I. Klokishner, B.L. Kushkuley, Chem. Phys. 166 (1992) 97.
[23] S.I. Klokishner, B.S. Tsukerblat, B.L. Kushkuley, New J. Chem. 17 (1993) 43.
[24] S.I. Klokishner, B.S. Tsukerblat, B.L. Kushkuley, Phys. Lett. A 179 (1993) 429.
[25] Y.E. Perlin, B.S. Tsukerblat, In: Y.E. Perlin, M. Wagner (eds.), The Dynamical Jahn-Teller Effect in Localized Systems, North-Holland, Amsterdam, 1984, p. 251.
[26] B.S. Tsukerblat, S.I. Klokishner, B.L. Kushkuley, Chem. Phys. 166 (1992) 97.
[27] S.I. Klokishner, J. Linares, F. Varret, J. Phys.: Condens. Matter 13 (2001) 595.